Journal of Materials Chemistry B

ROYAL SOCIETY OF CHEMISTRY

PAPER

View Article Online
View Journal | View Issue

Cite this: J. Mater. Chem. B, 2024, 12, 8662

Sustainable, aqueous exfoliation of MoS_2 *via* bio-inspired avenues†

Le Nhan Pham,‡§[a] Yuliana Perdomo,§[b] Joseph M. Slocik,[c] Rahul Rao,[c] Tiffany R. Walsh ¶*[a] and Marc R. Knecht ¶*[bd]

Two dimensional (2D) nanosheets of MoS_2 were succesfully produced by an exfoliation process in aqueous media with the support from peptides and sonication. The exfoliation process assisted by uncapped MoSBP1 peptides was found to have enhanced efficiency in comparison to the capped counterpart. MoS_2 nanosheets obtained using uncapped MoSBP1 have thinner structures containing one layer of MoS_2, while in capped version of peptides, MoS_2 nanosheets tend to form multilayer (up to 4) structures of exfoliated sheets. Molecular dynamics simulations indicate that inter-sheet gaps generated by sonication in MoS_2 nanostacks cannot be maintained by water only; the gaps closed after ~11 ns. Both capped CMoSBP1 and uncapped MoSBP1 were seen to spontaneously insert into the gap in nanostacks of MoS_2 and they can ultimately maintain the inter-sheet gap for longer (≥20 ns). Potential of mean force profiles for the association of two MoS_2 nanosheets decorated with CMoSBP1 and MoSBP1 versions of peptides revealed that uncapped MoSBP1 peptides provide good protection from MoS_2 nanosheet re-unification. Such protection can prevent the nanosheets from reassociation and subsequent aggregation, whereas the capped CMoSBP1 peptides can offer protection, but over a shorter range. These simulation results could explain the experimental observation of greater efficiency of exfoliation in uncapped MoSBP1 peptides.

Received 24th May 2024,
Accepted 29th July 2024

DOI: 10.1039/d4tb01127a

rsc.li/materials-b

Introduction

Transition metal dichalcogenides (TMDs) in a hexagonal structure (2H) feature a plane of metal atoms sandwiched between the two chalcogens and exhibit semiconductive and luminescent properties.[1–3] The well-defined band gap of the TMD materials allows for a wide range of applications, including their use in electronics and energy storage. To fully explore their potentially transformative application, the ability to sustainably access these two dimensional (2D) materials must be identified that allows for the acquisition of high quality structures with minimal defects.

One TMD that has been extensively studied for its electronic properties is MoS_2. Bulk MoS_2 has an indirect band gap of ~1.2 eV;[4] however, monolayer MoS_2 exhibits a direct band gap of ~1.8 eV.[5] Additionally, monolayer MoS_2 has displayed a significant electric field effect,[6] and its charge carrier mobility at room temperature has been determined to be between 0.5–2 $cm^2\ V^{-1}\ s^{-1}$.[7,8] Although the carrier mobility for MoS_2 is substantially less than that of graphene ($2 \times 10^5\ cm^2\ V^{-1}\ s^{-1}$),[8] this material promises more capabilities due to its finite band gap, which can be used at higher temperatures, power, and voltage.

To achieve MoS_2 nanosheets, liquid-phase exfoliation of the bulk stacked structure has been used.[9] During exfoliation, defects such as sulphur vacancies may occur, which can be used to covalently functionalize the surface through ligand attachment.[10] Unfortunately, such defects and functionalization can lead to diminished electronic properties. An ideal approach to overcome the negative effects of covalent ligand attachment is through the use of surface passivants that non-covalently adsorb onto the MoS_2 surface. Recently, Chen and co-workers have identified a peptide that non-covalently binds to MoS_2, which was termed MoSBP1 (YSATFTY).[11] Examination of both the native peptide and the end-capped version (acylated N-terminus and amidated C-terminus, Scheme 1) demonstrated MoS_2 surface binding through atomic force microscopy (AFM) and molecular dynamics (MD) simulation.[11] From the AFM analysis, the MoSBP1 peptide appeared to form an elongated linear structure on HOPG, a graphene surrogate, and MoS_2,

[a] Institute for Frontier Materials, Deakin University, Geelong 3216 VIC, Australia. E-mail: tiffany.walsh@deakin.edu.au
[b] Department of Chemistry, University of Miami, Coral Gables, FL 33146, USA. E-mail: knecht@miami.edu
[c] Air Force Research Laboratory, Wright-Patterson Air Force Base, Ohio 45433, USA
[d] Dr. JT Macdonald Foundation Biomedical Nanotechnology Institute, University of Miami, Miami, FL 33136, USA

† Electronic supplementary information (ESI) available. See DOI: https://doi.org/10.1039/d4tb01127a

‡ Current address: Flinders Institute for Nanoscale Science & Technology, College of Science & Engineering Flinders University.
§ These authors contributed equally.
¶ These authors contributed equally.

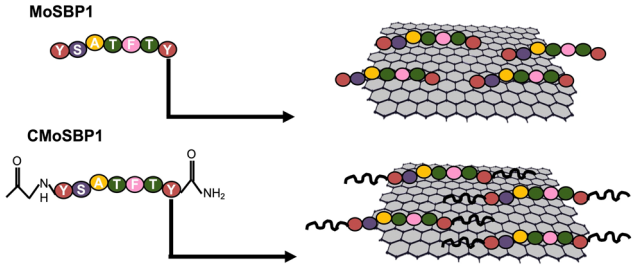

Scheme 1 MoSBP1 peptide sequences without (top) and with (bottom) end group capping.

showing preferred growth along the (100) facet of MoS_2. Although such results demonstrate that the MoSBP1 peptide binds to the MoS_2 surface, its use to generate high quality individual sheets was not assessed.

Hexagonal structured TMDs, such as MoS_2, have been exfoliated through sonication in water or organic solvents.[12–14] Typically, the exfoliation process requires the presence of ligands to stabilize and prevent the reassociation of individual exfoliated sheets back into their bulk stacked arrangement.[15] Peptides are viable bio-based ligands that can be used in aqueous media.[16,17] Additionally, peptide-assisted sonication is a low cost exfoliation method that produces little to no chemical waste, allowing for potentially sustainable routes to generate TMD nanosheets.[16] In this regard, peptides have been previously explored for aqueous sonication-based exfoliation of 2D materials such as graphene, in which the aromatic rings in the peptide residues can support π–π interactions with the surface.[18,19] Such non-covalent interactions can preserve the chemical and physical integrity of the 2D nanosheets and the electronic character of the surface.[20] That said, one study has reported the exfoliation of MoS_2 in liquid water after 8 h of sonication.[21] While interesting, the authors noted that the process led to extensive sheet fragmentation and damage (formation of mesoporous sheets). Furthermore, these authors reported subsequent colloidal stability was highly dependent on the formation of small fragments that were subjected to very high centrifugation rates.

While notable work has been done on peptide-based graphene exfoliation, only very limited studies have examined peptide-driven exfoliation of MoS_2 in aqueous media. Specifically, the exfoliation of MoS_2 was previously reported using cross-β-amyloid nanotubes that produced high quality 2-to-4 layered sheets.[22] While MoS_2 nanosheets were achieved, large, peptide-based structures were exploited for the exfoliation process. Further investigation of the effects of short, individual peptides for exfoliation may lead to new top-down approaches to generate MoS_2 sheets.

Herein, the exfoliation of individual sheets of MoS_2 from bulk systems is demonstrated using the MoSBP1 peptide where the effect of end capping is explored. The exfoliation process was studied both experimentally and *via* molecular simulations to provide atomically-resolved details of the interactions between the biomolecules and MoS_2 surface that drive the process. For exfoliation, the peptides and bulk MoS_2 were commixed in water and bath sonicated. The quality and quantity of MoS_2 nanosheets produced were compared between the parent MoSBP1 peptide and the capped variant (termed CMoSBP1). Once exfoliated, the isolated nanosheets were fully characterized *via* UV-vis, FT-IR and Raman spectroscopies, AFM, zeta potential analysis, and transmission electron microscopy (TEM). To complement the experimental observations, MD simulations were conducted to reveal details of the molecular mechanisms of the exfoliation process and colloidal stability of exfoliated MoS_2 nanosheets. From these results, single sheets of MoS_2 were prepared where the exfoliation efficiency was directly related to the peptide structures (capped *vs.* non-capped). These results demonstrate that direct and sustainable routes to MoS_2 production *via* sonication exfoliation is possible using bio-inspired approaches.

Experimental

Materials

Molybdenum(IV) sulfide powder, 99% trace metal basis, was procured from Beantown Chemical. MoSBP1 and CMoSBP1 peptides were obtained at >99% purity from Genscript. All chemicals were used as received. Ultrapure Milli-Q water (18.2 MΩ cm^{-1}) was used throughout the studies.

MoS_2 exfoliation

Peptide solutions were prepared by adding 0.5 mg of peptide (either CMoSBP1 or MoSBP1) to 5 mL of water in a 20.0 mL borosilicate glass vial. The solution was vortexed for 1 min, after which 25 mg of bulk MoS_2 powder was added to the vial and vortexed for an additional 1 min. The vials were then placed in the bath sonicator (Bransonic M2800) at the identified location of maximum sonication intensity and sonicated for 6 h.[18] The water level in the sonicator was monitored and refilled every 30–40 min, as needed. Once complete, the solutions were subsequently transferred to 50.0 mL Eppendorf centrifuge tubes and centrifuged for 1 h at 25 °C at a speed of 3000 rpm. The supernatant was finally decanted for further characterization.

MoS_2 characterization

UV-Vis analysis of the exfoliated MoS_2 was performed on an Agilent 8453 spectrometer with a 1 cm optical path length quartz cuvette. Zeta potential studies were conducted using a Malvern Zetasizer Nano S at 25 °C. The exfoliated solutions were lyophilized and FTIR was completed using a PerkinElmer Frontier FT-IR spectrometer. Raman spectroscopic analysis was performed with a Renishaw inVia Raman microscope. A gold-coated glass slide was dropcast with the exfoliated MoS_2 solution and Raman spectra were collected using 514.5 nm excitation at low laser powers (few μW). For the TEM studies, 5–10 μL of the exfoliated nanosheet solution was drop cast onto a lacey carbon-coated, 200 mesh copper TEM grid, purchased from EM Science. The samples were dried overnight in a desiccator and examined using an FEI C_s-corrected Titan TEM microscope operated at 300 kV. AFM images were obtained by drop casting 20 μL of the exfoliated solution onto a silicon wafer, which was allowed to dry

for 3 h. The surface was subsequently lightly rinsed with water, dried with air, and then placed in a desiccator overnight. AFM analysis was performed using a dimension 3100 model microscope (Veeco) operating in tapping mode. X-Ray photoelectron spectroscopy (XPS) was performed using an M-PROBE surface science XPS spectrometer with charge neutralization. Samples were prepared by dropcasting 2 μL of an aqueous suspension onto a polished silicon wafer and air dried. High resolution XPS scans were obtained using 0.01 eV steps and averaged over 50 scans.

Molecular dynamics simulations

To explore the exfoliation process of MoS_2 nanosheets facilitated by peptides, two types of MD simulation approaches were used. The first sought to investigate the exfoliation of the nanosheets from a stack of MoS_2 sheets in liquid water under sonication conditions. The second type sought to evaluate the post-sonication colloidal stability of MoS_2 nanosheets decorated with peptides in aqueous media at room temperature (300 K).

In the first approach, a stack of 10 MoS_2 sheets of dimension $\sim 5 \times 5$ nm in liquid water was modelled featuring an expanded inter-sheet gap between the top sheet and the remainder of the stack, to mimic gap expansion during sonication. Under these conditions, the spontaneous ingress of peptides into this expanded gap was investigated. An example simulation setup is provided in Fig. 1a and b. In addition, MD simulations were used to evaluate the maintenance of this expanded gap as a function of time in the presence of pre-inserted peptides, compared with the stability of the gap in the absence of peptides. Both sets of simulations were performed at a temperature of 340 K in the NVT ensemble.

In the second approach, the system comprised two identical peptide-decorated (either CMoSBP1 or MoSBP1) MoS_2 sheets (34 peptides per sheet, 17 per side) that were initially arranged face-to-face along the *z*-axis (perpendicular to the sheet plane), where the distance between centers of the two sheets was 5 nm. The system was solvated with sufficient water molecules. An example of this configuration is provided in Fig. 1c. A total of 55 configurations were used in the umbrella sampling simulations at 300 K in the NVT ensemble, for which the two sheets were drawn closer together and the reaction coordinate for the free energy profile was defined by the vertical inter-sheet distance. Each umbrella sampling window was simulated for 100 ns. The resultant free energy profile describing the approach of the two peptide-decorated sheets can indicate the general stability of the resultant suspension.

All MD simulations were done using Gromacs 2021.2.[23] The MoSu-CHARMM[24,25] force field was employed to describe interaction between water (TIPS3P[26,27]) and MoS_2 surface, and between peptides and the MoS_2 nanosheets. Parameters used to describe the internal bonded structures[28] of the MoS_2 sheets and the MoS_2 inter-sheet interactions were adopted from literature.[29] Full details of the simulations are given in the ESI.†

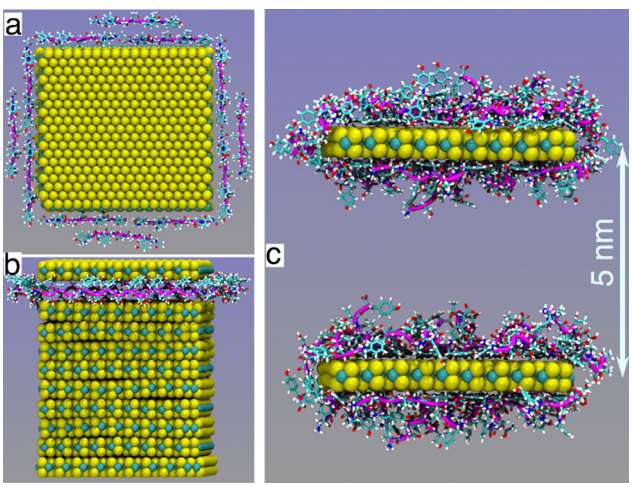

Fig. 1 (a) Top view and (b) side view of initial arrangement of peptides used for modelling spontaneous insertion of peptide chains into the MoS_2 gap. (c) Example of simulation configuration to probe the stability of MoS_2 nanosheets decorated with peptide chains. Water molecules not shown for clarity.

Results and discussion

Exfoliation analysis

To drive peptide-assisted MoS_2 exfoliation, a low-energy bath sonication approach was adapted from prior studies employed for graphene exfoliation.[18,30] Briefly, an aqueous solution of the two peptides (MoSBP1 and CMoSBP1, 5 mL at 0.1 mg mL^{-1}) was prepared where the mixture was sonicated for 2 min to facilitate peptide dissolution. This step was important due to the limited solubility of the capped CMoSBP1 biomolecule. Once dissolved, 50 mg of bulk MoS_2 powder was added to the mixture, and the system was sonicated in a bath sonicator for 6 h. It is important to note that the exfoliation efficiency was highly sensitive to the position of the vial in the bath sonicator; the reaction must be positioned at the point of maximum sonication in the system, as previously demonstrated.[18,31] Once the exfoliation process was complete, the reaction mixture was centrifuged to remove any remaining bulk MoS_2 powder where the exfoliated samples remain suspended in the supernatant. These materials were subsequently characterized.

UV-Vis analysis enabled the comparison of MoS_2 exfoliation efficiency conferred by the MoSBP1 and CMoSBP1 peptides, (Fig. 2a). For comparison, images of the exfoliation supernatant are present in the inset of Fig. 2a, demonstrating a yellow solution for the reactions where peptides were present. This colour, which was different than for the bulk powder that is grey, is consistent with prior MoS_2 exfoliation systems.[9] A separate control exfoliation, in which bulk powder was sonicated in water in the absence of any biomolecule, was performed under the same sonication conditions. For the peptide-driven reactions, nearly identical UV-vis spectra were observed with four distinct peaks at $\sim$390, $\sim$450, $\sim$610, and $\sim$660 nm. The two peaks at $<$500 nm correlated to the direct transition from deep within the valence band to the conductive band at the *M* point in the Brillouin zone.[32–34] The two smaller

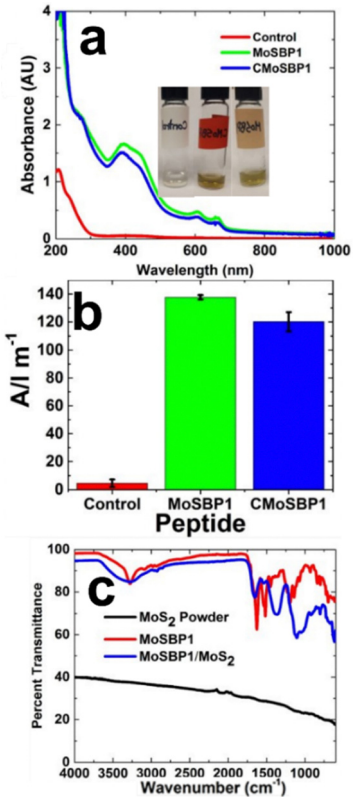

Fig. 2 Spectroscopic analysis of peptide-driven MoS_2 exfoliation. (a) UV-Vis spectra of the exfoliated materials where the insert displays images of the reaction systems. (b) Comparison of the absorbance values at 348 nm for the reactions in panel (a). (c) FT-IR analysis of the exfoliated materials achieved using the indicated peptide.

peaks located at >500 nm were consistent with the excitation transition of the *K* point.[35–38] The presence of these peaks indicated successful peptide-assisted exfoliation of 2H MoS_2 sheets with both CMoSBP1 and MoSBP1. This is significant because previously reported biomolecule-based aqueous exfoliation of MoS_2 required the formation of peptide nanotubes to produce the MoS_2 nanosheets,[22] whereas this was successfully accomplished here using a seven residue peptide.

In the absence of peptide, this system did not exhibit any significant absorbances at wavelengths >300 nm; however, there were minor, broad absorbances, which may be attributed to MoS_2. As previously shown, modest MoS_2 exfoliation can be achieved in water.[9,39] That said, comparison of the spectra achieved for the control with the two peptide-based systems clearly demonstrated enhanced nanosheet production in the presence of both CMoSBP1 and MoSBP1. To compare the exfoliation efficiency, the absorbance intensity at 348 nm was compared between the three samples (Fig. 2b). This wavelength was chosen because, at this point, there is a consistent minimum that is not affected by the varying layers of MoS_2. Other points in the spectra may shift due to defects in the sheets, conformational differences, or sheet thickness; thus, observing the absorbance at 348 nm provides a uniform measurement for quantifying concentration. From this comparison, the control reaction intensity was substantially lower than for the reactions with the peptides, indicating negligible MoS_2 nanosheet exfoliation. For the peptide-driven systems, a slight increase in the absorbance for the MoSBP1-exfoliated system was observed over the CMoSBP1-based reaction, suggesting enhanced MoS_2 sheet production from the uncapped peptide. This might in part be attributed to the relatively greater solubility of the MoSBP1 peptide in water compared to CMoSBP1. This relative difference in solubility of the uncapped and capped variants in which the uncapped version is more soluble, may affect the exfoliation efficiency.

The success of this exfoliation process requires successful outcomes for two successive stages: first, the sheets must be able to be detached from the bulk material during sonication, and second, these detached sheets must be prevented from re-associating once the sonication process is completed. Although the sonication experiments can evaluate the overall success of exfoliation *via* observation of the resultant colloidal suspension, it is challenging for experiment to directly verify the specific details of these two stages. However, MD simulations can provide atomic-scale insights into each stage of this process.

MD simulation data show that bare 2D nanosheets (*i.e.*, in the absence of peptide) of MoS_2 were unlikely to maintain long-term colloidal stability in liquid water. This was probed *via* simulation of the MoS_2 stack with an initial expanded gap between the top layer and the remainder of the stack (Fig. S2a, ESI†). This was done to capture the gap expansion due to sonication in the experiments. The gap collapse started after an average time of ~7 ns of simulation, and it completely closed after ~9 ns of simulation. The mechanism of gap collapse took place in two steps. In the initial step, the top sheet of MoS_2 displaced downward by around half the original gap distance (~5 Å), corresponding to expulsion of one layer of water inside the gap. This first stage took a total ~100 ps. Thereafter, the second water layer was expelled in the next ~1 ns. In total, after ~9 ns the expanded gap was completely closed. The whole process of gap closure is illustrated in Fig. S4a, ESI.† This result indicates that individual 2D nanosheets of MoS_2 will aggregate with the MoS_2 stack in pure water. These simulated mechanism data are consistent with the experimental results of the control sample and can explain why MoS_2 cannot be sufficiently exfoliated *via* sonication in liquid water alone.

In contrast, with the presence of MoSBP1 peptide chains in the solvent, the spontaneous insertion of these biomolecules into the expanded gap was observed almost immediately (within ~2 ns for the vertical initial arrangement, Fig. 3). For the parallel initial arrangement (Fig. S4b, ESI†), the spontaneous insertion took only ~1.3 ns, which is two times shorter than for the vertical initial arrangement of MoSBP1 peptides. The longer ingress time seen for the initial vertical arrangement is understandable due to steric challenges of the ingress of the vertically arranged peptides. As a result, the gap was maintained during the simulation (20 ns) following the spontaneous ingress of the peptides, although by the end of simulation not all chains had entered the gap (Fig. 3). In addition, the capped peptide (CMoSBP1) also supported spontaneous peptide

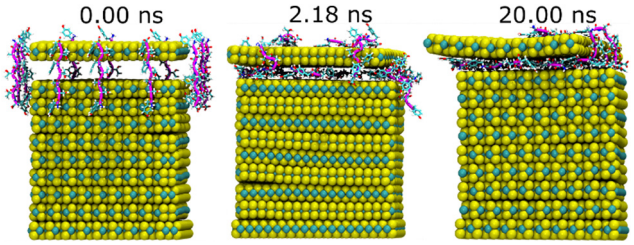

Fig. 3 Snapshots of spontaneous insertion of MoSBP1 peptides into the gap. The initial arrangement of MoSBP1 is vertical to the MoS_2 nanosheet plane. Simulation-averaged insertion times shown. Water molecules not shown for clarity.

ingress, again maintaining the expanded gap for the duration of the 20 ns simulation. These simulation results are consistent with the experimental exfoliation efficiency data represented by the UV-vis data presented in Fig. 2 where both capped and uncapped peptides were able to exfoliate bulk MoS_2.

To experimentally confirm the interaction between the peptide and MoS_2, FT-IR spectroscopy was employed. Fig. 2c presents the FT-IR spectra of an aqueous solution (MoSBP1 – red spectrum), bulk MoS_2 (black spectrum), and the MoSBP1-exfoliated MoS_2 nanosheets (blue spectrum). The results achieved using the capped CMoSBP1 peptide are presented in the ESI,† Fig. S5. For the bulk MoS_2 powder, no significant stretching bands were observed over the wavelengths of interest, as anticipated. Conversely, the MoSBP1 peptide solution displayed a peak at $\sim$3350 cm^{-1} for the symmetrical stretching of the N–H vibrations, as well as a peak at 3280 cm^{-1} for antisymmetric stretching. The peak at 1590 cm^{-1} arises from the N–H bending, while the other peak at around 1650 cm^{-1} is for the C═O stretching, both arising from the amide backbone of the biomolecule. When examining the peptide-capped MoS_2 exfoliated sheets, the peaks for the peptide generally remained in the sample; however, their intensities were diminished. This suggests that the peptides were indeed adsorbed to the nanosheet surface to facilitate exfoliation and colloidal stabilization in water. Zeta potential analysis of the exfoliated sheets was also conducted (Fig. S6, ESI†), which gave rise to surface charges of -32 and -35 mV for MoSBP1- and CMoSBP1-decorated materials, respectively. The control exhibited a much lower charge at around -20 mV.

To confirm the structures of the isolated materials, the peptide-assisted exfoliated sheets were imaged using TEM, as presented in Fig. 4. The interplanar spacing for MoSBP1 exfoliated sheet was found to be 0.255 nm. The darker contrasted areas in Fig. 4a and b, are multiple sheets layered over one another. Fig. 4b gives a more in-depth image of possibly two MoS_2 sheets on top of one another and shows overlaid crystalline structures of multiple sheets were observed, which resulted in the linear pattern in the image and the darker contrast. The TEM with CMoSBP1 exfoliated sheets showed multiple layers of MoS_2, as seen in Fig. 4c. In this figure, there were materials that show distinct structures of between 3–4 layers. The same can be seen in Fig. 4d, where there is a single long structure that has four distinct layers. This suggests that

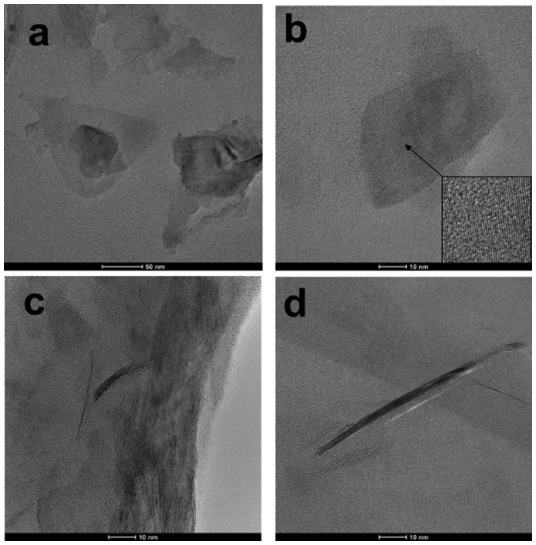

Fig. 4 TEM analysis of the exfoliated materials using the (a) and (b) MoSBP1 and (c) and (d) CMoSBP1 peptides. Scale bars are 50 nm in part (a) and 10 nm in parts (b)–(d).

the CMoSBP1 may be less efficient at exfoliation compared to the parent, uncapped peptide.

As observed from the UV-vis and TEM analyses, the exfoliation processes with the capped peptide, CMoSBP1, had less exfoliation efficiency. In addition, the exfoliated nanosheets tended to form thicker structures consisting of three to four MoS_2 layers in comparison to those obtained from the exfoliation processes assisted with the uncapped peptide MoSBP1. To investigate this further, umbrella sampling MD simulations were performed to estimate the free energy of interaction of MoS_2 nanosheets, decorated with capped and uncapped peptide chains. The potential of mean force (PMF) profiles for the unification of two peptide-decorated MoS_2 sheets in liquid water are given for each case in Fig. 5.

The PMF profiles from the umbrella sampling simulations for MoS_2 nanosheets decorated with capped and uncapped peptides can give more insights into the resultant colloidal stability following exfoliation. Two key interaction behaviors can be observed from these two PMF profiles. The first can be seen through the magnitude of repulsive forces once the two decorated sheets approach each other. Two MoS_2 nanosheets decorated with uncapped peptides MoSBP1 repel each other with approximately double the strength compared with nanosheets decorated with the capped version of peptides CMoSBP1 when the two nanosheets were close to each other (at an inter-sheet distance of $\sim$1.5 nm). A second distinction between the capped and uncapped systems was found in the repulsive inter-sheet region between two MoS_2 nanosheets. The MoS_2 nanosheets with uncapped MoSBP1 peptides started to repel each other at an inter-sheet distance of $\sim$4.0 nm. Once the inter-sheet distance reduced $\sim$2.5 nm, the repulsive force started to exponentially increase and reached $\sim$80 kJ mol^{-1} at 1.5 nm. On the other hand, MoS_2 nanosheets decorated with capped peptides are not as repelled for inter-sheet distances

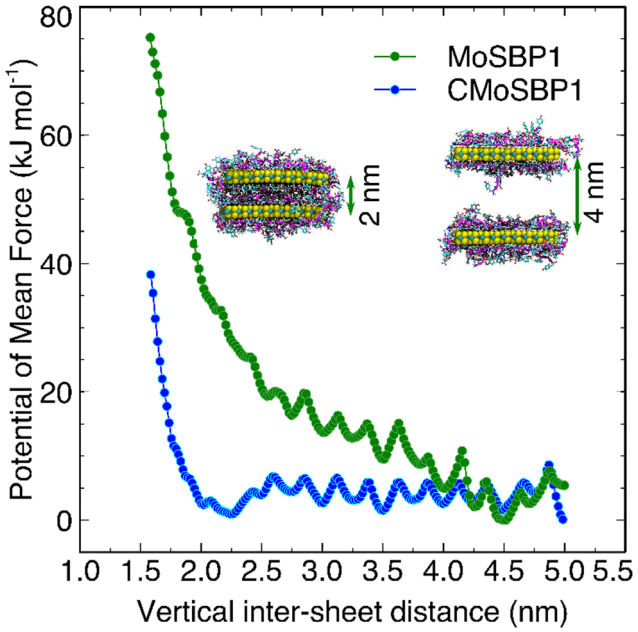

Fig. 5 PMF associated with the reunification of two MoS_2 nanosheets decorated with capped (blue) CMoSBP1 and uncapped (green) MoSBP1 peptides. The vertical inter-sheet distance is the distance between the two centers of mass of the MoS_2 nanosheets, excluding all attached peptides.

from 2.2 to 4.0 nm; the repulsion was observed for inter-sheet distances of less than ~2.2 nm. Both a greater repulsive force and longer-distance repulsion observed in MoS_2 nanosheets decorated with uncapped MoSBP1 peptides indicate that these decorated sheets were inhibited from reunification, whereas those covered with the capped peptides CMoSBP1 may approach each other as close as a distance of ~2.2 nm. Such a close approach can allow more opportunities for aggregation if peptides are slightly detached from the decorated sheets. The PMF profiles are consistent with the experimental outcomes, specifically that CMoSBP1 confers less efficiency in the exfoliation of MoS_2 stacks, and that exfoliated MoS_2 nanosheets in the capped peptide system yield multiple layers of MoS_2 (up to four layers, Fig. 4d).

Analysis of water inside the gap between the two approaching sheets revealed that MoS_2 nanosheets decorated with uncapped peptides MoSBP1 were more hydrated in comparison to those decorated with the capped version of the peptides (Fig. S7, ESI†). At the closest inter-sheet distance of ~1.52 nm, the nanosheets with uncapped peptides have ~20% more water molecules in the space between the MoS_2 nanosheets than those decorated with capped peptides (509 *vs.* 427 water molecules). This result is understandable because the uncapped peptides have charged termini (NH_3^+ and COO^-), whereas the termini of CMoSBP1 chains are capped with the hydrophobic CH_3 groups. As a result, the MoS_2 nanosheets exfoliated with MoSBP1 peptides are better solvated, and it is possible this additional solvation contributes to the enhanced colloidal stability in the uncapped case.

The umbrella sampling simulations suggest that uncapped MoSBP1 peptides can make contact with their counterpart attached to the opposite MoS_2 sheets at a longer distance of inter-sheet gaps. At the inter-sheet distance of ~3.10 nm, the uncapped peptide chains can make contact with their counterparts on the opposite MoS_2 nanosheet, whereas in the capped CMoSBP1 system, the surface-attached chains on the two sheets remain distant (Fig. S9a and b, ESI†). Quantitatively, at the inter-sheet distance of ~3.1 nm, the mass density of uncapped MoSBP1 peptides at the mid-point of the gap between the two MoS_2 nanosheets is ~5.0 kg m^{-3}, while this value of capped CMoSBP1 ones is ~0 kg m^{-3} (red line in the green dashed circle, Fig. 6a). The capped CMoSBP1 peptides started to make contact at a shorter gap distance (~2.45 nm, Fig. S9d, ESI†). This can be observed through the non-zero mass density (~5.0 kg m^{-3}) of capped peptides at this mid-point shown in Fig. 6b (red line in the green dashed circle), while the mass density of uncapped peptides (blue line) is ~15 kg m^{-3}. This is three times higher than that of the capped peptides. In general, for the same inter-sheet separation, uncapped peptides were more likely to be present at the mid-point region, and hence could better protect MoS_2 nanosheets from aggregation. The onset of this protection also occurs at greater inter-sheet vertical separations (3.10 ns *vs.* 2.45 nm). Together with stronger solvation, as discussed above, protection from aggregation at greater inter-sheet vertical separations, along with the higher density of uncapped peptides at the inter-sheet spacing midpoint, is consistent with more stable suspensions of MoS_2 nanosheets decorated with uncapped MoSBP1 chains.

Additionally, analysis of residue contact time can reveal how individual residues of peptides remain in contact with the MoS_2 nanosheets. The data obtained at two gap distances of 3.10 and 2.45 nm (Table S3, ESI†) show that the charged groups NH_3^+ in the uncapped peptides spend more time, on average, in the solution (~70% of time), while the charge-neutral groups of the acylated capped CMoSBP1 spend more time in contact with the MoS_2 sheets (60% of time). In contrast, the two terminal groups COO^- and NME of the uncapped and capped peptides, respectively, were in contact with the MoS_2 surface ~40% of time. From the distribution of strongest-contact residues (at the inter-sheet separations of 3.10 and 2.45 nm) with >80% contact time, visualized in Fig. S11, ESI,† it is evident that on the upper sheet the number of anchor residues in the capped CMoSBP1 peptides is higher than those in the uncapped MoSBP1 system (at 3.10 nm: 3 and 0; at 2.45 nm: 3 and 0, respectively). On the lower sheet, at the inter-sheet distance of 3.10 nm, a solo residue Tyr1 in the uncapped system, and the residue Tyr7 in the capped system, were found to be the anchor residues (Fig. S11, ESI†), but the acylated terminal group of the capped peptides has 71% contact time, resulting in both ends of the capped peptides most likely being in contact with the MoS_2 surface most of the time. A similar situation can be observed in the lower sheet at the inter-sheet distance of 2.45 nm for the capped peptides. Here the terminal acylated group (52% contact time) and the strongest-contact residue (Phe5) were in contact most of the time, whereas the uncapped peptides tended to have more freedom at one end

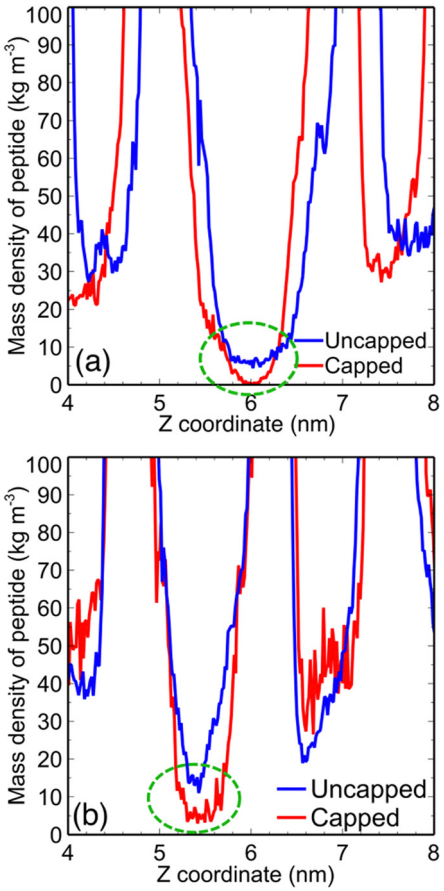

Fig. 6 Mass density of peptides along the *Z* coordinate axis (perpendicular to the sheet plane) measured at the inter-sheet gap distances of (a) 3.10 nm and (b) 2.45 nm. The densities in the middle regions are circled in green dashed lines.

(from residues Thr4 to Tyr7). In this case, the Tyr7 residue of the capped peptides also had a high contact time (79%, Table S3, ESI†) and is proposed to contribute to intensive contact of the capped peptides to the MoS_2 surface as well. The lesser average contact time of the uncapped peptide residues and terminal groups (to an extent) is proposed to explain why uncapped peptides can make contact with peptides on the opposite MoS_2 nanosheet at a greater inter-sheet separation, resulting in higher mass density in the midpoint region of the inter-sheet spacing.

With confirmation of the stability of the exfoliated materials, the thickness of the MoSBP1-exfoliated MoS_2 sheets was further examined *via* AFM, as shown in Fig. 7. Since the TEM data indicated that the CMoSBP1 peptides were not as efficient at MoS_2 exfoliation, additional AFM analysis was not conducted on these materials. Fig. 7a specifically presents the AFM image of the MoSBP1-exfoliated materials. Statistical analysis of >100 nanosheets was conducted (Fig. 7b), where a bimodal height distribution was noted with two maxima at 1.8 ± 0.5 and 3.7 ± 0.5 nm. Such values suggest that MoS_2 sheets from one to four layers were predominantly in the sample.

Raman spectra from both capped and uncapped peptide decorated MoS_2 flakes were measured using an excitation

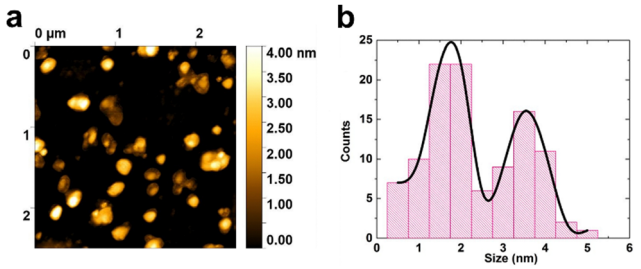

Fig. 7 AFM analysis of the MoSBP1-exfoliated MoS_2 materials. Part (a) presents the AFM image, while part (b) presents the height analysis of >100 measurements.

wavelength of 514.5 nm. Multiple spectra were collected from drop-casted flakes and average spectra are shown in Fig. 8. Both MoSBP1 and CMoSBP1 exhibit peaks at ~ 382 and ~ 406 cm^{-1}, corresponding to the in-plane and out-of-plane vibrational modes of MoS_2 (E_{2g} and A_{1g}, respectively, as shown in the inset in Fig. 8).[40] The frequency difference between the two peaks is ~ 24 cm^{-1}, indicative of few-layer MoS_2, and reflects aggregation of the flakes upon drying within the drop-casted areas.[40] The spectra from the two samples do exhibit some differences. Firstly, Voigt lineshape fitting of the MoS_2 peaks (Fig. S12, ESI†) revealed the MoSBP1 peaks to be slightly narrower than the CMoSBP1 peaks ($\sim 1 \pm 0.26$ and 0.5 ± 0.17 cm^{-1} for the E_{2g} and A_{1g} peaks, respectively). The lower peak widths in the MoSBP1 indicates a higher crystallinity compared to CMoBPS1. Additionally, Raman spectra collected at higher frequencies reveal peaks (between 1200–1750 cm^{-1}) corresponding to the organic peptide coatings. The higher intensity of the carbon peaks in the MoSBP1 may be attributed to a higher coverage of the uncapped peptides on the MoS_2 surface and support the observations in the PMF profiles (*i.e.*, reduced aggregation in the uncapped MoSBP1).

Due to the non-covalent nature of the peptide–MoS_2 interaction, this peptide coverage is not expected to be static. Previous estimates of the binding free energy of amino acids

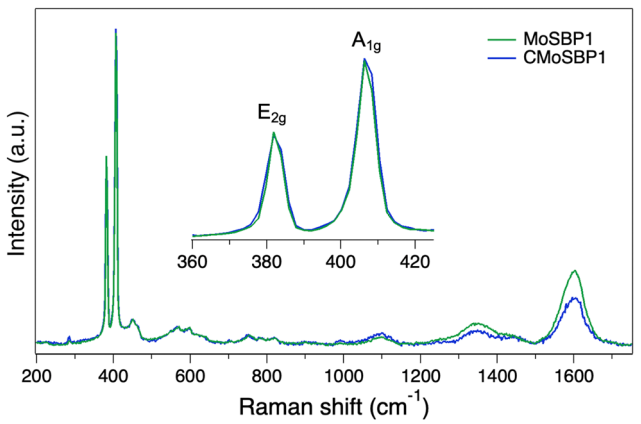

Fig. 8 Raman spectra collected (using 514.5 nm excitation) from MoSBP1 and CMoSBP1-exfoliated MoS_2. The plotted spectra are averages of spectra collected from several spots on dropcasted samples. The inset shows the MoS_2 Raman peaks.

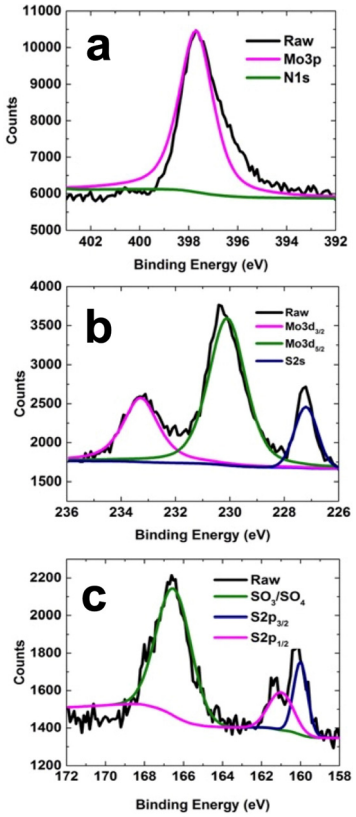

Fig. 9 XPS analysis of the MoSBP1-exfoliated MoS_2 materials for the (a) Mo 3p, (b) Mo $3d_{3/2}$ and Mo $3d_{5/2}$, and (c) S $2p_{1/2}$ and $2p_{3/2}$ peaks.

on the MoS_2 surface suggest that the binding affinities of the MoSBP1-based peptides are of the order of 20–30 kJ mol^{-1}.[24] Therefore it is expected that the peptides adsorbed on the surface could be exchanging with peptides or other molecules in solution under standard temperature and pressure conditions over reasonable timescales.

Finally, XPS analysis of the MoSBP1-exfoliated MoS_2 materials was performed, which confirmed the generation of the peptide-capped materials. Fig. 9a demonstrates the presence of Mo^{4+}, with a deconvoluted 3p peak at 398 nm, and the presence of nitrogen from the peptide at 400.5 nm (1s peak).[8,41] Note that the peak associated with nitrogen is quite low in intensity due to its low concentration with respect to Mo in the sample. At 230 and 233 eV, the binding energy of the 3d orbital for Mo^{4+} in 2H MoS_2 was also observed, arising from the $3d_{3/2}$ and $3d_{5/2}$, respectively (Fig. 9b).[8,41] Additionally, the peak at 227 eV originates from the 2s orbital of the sulphur atoms of MoS_2. In addition, Fig. 9c displays the peaks for the $2p_{1/2}$ (161 nm) and $2p_{3/2}$ (160 nm) spin orbitals of sulphur.[8,41] Interestingly, an unexpected peak was observed at 167 eV, which likely arises from oxidation of the sulphur atoms in MoS_2 to a sulfoxide. Previous studies of MoS_2 exfoliation have demonstrated such oxidation can occur to generate either SO_3 or SO_4.[8,42,43]

Using the method demonstrated herein, peptide-assisted exfoliation of MoS_2 is achieved under sustainable conditions (*e.g.*, room temperature, energy efficient, and aqueous solvent). A variety of different methods have been previously exploited to exfoliate MoS_2, including sonochemical, electrochemical, and mechanical methods.[44,45] While many methods have positive features such as high yields, exfoliation efficiency, material size, *etc.*, many of them require the use of organic solvents, complicated apparatuses, or covalent MoS_2 surface functionalization. For instance, Quirós-Ovies *et al.* recently exploited microwave-based heating for MoS_2 exfoliation, which demonstrated high yields of the nanosheets; however, this method requires a unique microwave-based system and exploited organic solvents for exfoliation.[46] In separate work, Bissett and colleagues electrochemically exfoliated MoS_2 to generate electrocatalytically active materials.[47] The approach is intriguing, but again requires organic solvents and an electrochemical set up for the reaction. Iamprasertkun and coworkers were able to demonstrate an aqueous-based exfoliation process for MoS_2 *via* sonication where the addition of *N*-methyl-2-pyrrolidone (NMP) was used to enhance the process.[48] Interestingly, maximum exfoliation was observed with 35 : 65 ratio of water : NMP as the solvent, again requiring a mostly organic medium to drive the process. In addition, at high water solvent concentrations (>66.7%), MoO_3 was observed in this system. While good material yields are achieved, organic solvents are again required where high aqueous solvents led to material oxidation.

Conclusions

MoS_2 materials have been exfoliated in aqueous media with the support of a MoS_2-binding peptide and sonication. Both capped and uncapped MoSBP1 were demonstrated to facilitate the exfoliation process, in which uncapped peptides were found to be more efficient in exfoliating the MoS_2 into smaller structures. The exfoliated nanosheets were found to have different morphologies based upon the capped *vs.* uncapped structure of the peptide, which likely arises from the interactions between the material and biomolecule. Molecular simulations of both the initial exfoliation process and the stability of the resultant exfoliated sheets in solution were consistent with the experimental data. Specifically, the simulations suggest that the presence of the peptides is critical for enabling the first step of the exfoliation mechanism by maintaining the expanded gap induced by sonication. Furthermore, the experimentally-observed differences in the exfoliated product for the capped and uncapped systems can in part be explained by the free energy profiles related to the reunification of peptide-decorated MoS_2 nanosheets. The lesser protection conferred by the capped peptides is likely due to the observation that the sheets decorated by capped peptides could approach relatively closer compared with their uncapped counterparts.

These findings provide a bio-based platform for the manipulation, organisation, and activation of MoS_2 materials in aqueous media. Such effects could prove to be highly important in the design of new nanoscale systems and devices that require surface conjugation on the MoS_2 materials without covalent

attachment or defect incorporation. Exploitation of this capability is currently under exploration.

Author contributions

L. N. P. and Y. P. contributed equally to this work. T. R. W. and M. R. K. contributed equally to this work.

Data availability

All data, both experimental and computational, is available upon request to the authors.

Conflicts of interest

There are no conflicts to declare.

Acknowledgements

This material was based upon work supported by the Air Force Office of Scientific Research, Grant FA9550-18-1-0329 and FA9550-23-1-0253. L. N. P. and T. R. W. thank the National Computing Infrastructure, Australia, for computational resources under the NCMAS scheme.

Notes and references

1 X. Chia, A. Y. S. Eng, A. Ambrosi, S. M. Tan and M. Pumera, *Chem. Rev.*, 2015, **115**, 11941–11966.
2 W. Zhai, Z. Li, Y. Wang, L. Zhai, Y. Yao, S. Li, L. Wang, H. Yang, B. Chi, J. Liang, Z. Shi, Y. Ge, Z. Lai, Q. Yun, A. Zhang, Z. Wu, Q. He, B. Chen, Z. Huang and H. Zhang, *Chem. Rev.*, 2024, **124**, 4479–4539.
3 G. H. Han, D. L. Duong, D. H. Keum, S. J. Yun and Y. H. Lee, *Chem. Rev.*, 2018, **118**, 6297–6336.
4 G. L. Frey, S. Elani, M. Homyonfer, Y. Feldman and R. Tenne, *Phys. Rev. B: Condens. Matter Mater. Phys.*, 1998, **57**, 6666–6671.
5 K. F. Mak, C. Lee, J. Hone, J. Shan and T. F. Heinz, *Phys. Rev. Lett.*, 2010, **105**, 136805.
6 J. Shi, L. Chen, M. Yang, Z. Mi, M. Zhang, K. Gao, D. Zhang, S. Su and W. Hou, *Curr. Appl. Phys.*, 2022, **39**, 331–338.
7 R. Fivaz and E. Mooser, *Phys. Rev.*, 1967, **163**, 743–755.
8 A. Ambrosi, Z. Sofer and M. Pumera, *Small*, 2015, **11**, 605–612.
9 A. Gupta, V. Arunachalam and S. Vasudevan, *J. Phys. Chem. Lett.*, 2016, **7**, 4884–4890.
10 Q. Jin, N. Liu, B. Chen and D. Mei, *J. Phys. Chem. C*, 2018, **122**, 28215–28224.
11 J. Chen, E. Zhu, J. Liu, S. Zhang, Z. Lin, X. Duan, H. Heinz, Y. Huang and J. J. De Yoreo, *Science*, 2018, **362**, 1135–1139.
12 U. Patil and N. M. Caffrey, *J. Chem. Phys.*, 2018, **149**, 094702.
13 E. P. Nguyen, B. J. Carey, T. Daeneke, J. Z. Ou, K. Latham, S. Zhuiykov and K. Kalantar-zadeh, *Chem. Mater.*, 2015, **27**, 53–59.
14 X. Hai, K. Chang, H. Pang, M. Li, P. Li, H. Liu, L. Shi and J. Ye, *J. Am. Chem. Soc.*, 2016, **138**, 14962–14969.
15 M. Jeong, S. Kim and S.-Y. Ju, *RSC Adv.*, 2016, **6**, 36248–36255.
16 T. R. Walsh and M. R. Knecht, *Bioconjugate Chem.*, 2019, **30**, 2727–2750.
17 T. R. Walsh and M. R. Knecht, *Chem. Rev.*, 2017, **117**, 12641–12704.
18 A. D. Parab, A. Budi, J. M. Slocik, R. Rao, R. R. Naik, T. R. Walsh and M. R. Knecht, *J. Phys. Chem. C*, 2020, **124**, 2219–2228.
19 R. Jin, N. Brljak, J. M. Slocik, R. Rao, M. R. Knecht and T. R. Walsh, *J. Mater. Chem. B*, 2024, **12**, 4824–4832.
20 H. Wang, W. Lv, J. Shi, H. Wang, D. Wang, L. Jin, J. Chao, P. A. van Aken, R. Chen and W. Huang, *ACS Sustainable Chem. Eng.*, 2020, **8**, 84–90.
21 H. Ma, Z. Shen and S. Ben, *J. Colloid Interface Sci.*, 2018, **517**, 204–212.
22 N. Kapil, A. Singh, M. Singh and D. Das, *Angew. Chem., Int. Ed.*, 2016, **55**, 7772–7776.
23 M. J. Abraham, T. Murtola, R. Schulz, S. Páll, J. C. Smith, B. Hess and E. Lindahl, *SoftwareX*, 2015, **1–2**, 19–25.
24 L. N. Pham and T. R. Walsh, *Chem. Sci.*, 2022, **13**, 5186–5195.
25 L. N. Pham and T. R. Walsh, *Chem. Commun.*, 2021, **57**, 3355–3358.
26 W. L. Jorgensen, J. Chandrasekhar, J. D. Madura, R. W. Impey and M. L. Klein, *J. Chem. Phys.*, 1983, **79**, 926–935.
27 E. Neria, S. Fischer and M. Karplus, *J. Chem. Phys.*, 1996, **105**, 1902–1921.
28 J. Liu, J. Zeng, C. Zhu, J. Miao, Y. Huang and H. Heinz, *Chem. Sci.*, 2020, **11**, 8708–8722.
29 V. Sresht, A. Govind Rajan, E. Bordes, M. S. Strano, A. A. H. Pádua and D. Blankschtein, *J. Phys. Chem. C*, 2017, **121**, 9022–9031.
30 A. D. Parab, R. Dureja, R. Rao, J. M. Slocik, R. R. Naik, T. R. Walsh and M. R. Knecht, *Langmuir*, 2021, **37**, 1152–1163.
31 L. I. Silva, D. A. Mirabella, J. Pablo Tomba and C. C. Riccardi, *Ultrasonics*, 2020, **100**, 105989.
32 D. Gopalakrishnan, D. Damien and M. M. Shaijumon, *ACS Nano*, 2014, **8**, 5297–5303.
33 J. A. Wilson and A. D. Yoffe, *Adv. Phys.*, 1969, **18**, 193–335.
34 W. Wilcoxon and S. Samara, *Phys. Rev. B: Condens. Matter Mater. Phys.*, 1995, **51**(11), 7299–7302.
35 V. Chikan and D. F. Kelley, *J. Phys. Chem. B*, 2002, **106**, 3794–3804.
36 J. P. Wilcoxon, P. P. Newcomer and G. A. Samara, *J. Appl. Phys.*, 1997, **81**, 7934–7944.
37 T. Wang, L. Liu, Z. Zhu, P. Papakonstantinou, J. Hu, H. Liu and M. Li, *Energy Environ. Sci.*, 2013, **6**, 625–633.
38 J. Kopaczek, M. P. Polak, P. Scharoch, K. Wu, B. Chen, S. Tongay and R. Kudrawiec, *J. Appl. Phys.*, 2016, **119**, 235705.

39 D. Sahoo, B. Kumar, J. Sinha, S. Ghosh, S. S. Roy and B. Kaviraj, *Sci. Rep.*, 2020, **10**, 10759.
40 A. Jawaid, D. Nepal, K. Park, M. Jespersen, A. Qualley, P. Mirau, L. F. Drummy and R. A. Vaia, *Chem. Mater.*, 2016, **28**, 337–348.
41 Z. Lin, Y. Liu, U. Halim, M. Ding, Y. Liu, Y. Wang, C. Jia, P. Chen, X. Duan, C. Wang, F. Song, M. Li, C. Wan, Y. Huang and X. Duan, *Nature*, 2018, **562**, 254–258.
42 Q. D. Truong, M. Kempaiah Devaraju, Y. Nakayasu, N. Tamura, Y. Sasaki, T. Tomai and I. Honma, *ACS Omega*, 2017, **2**, 2360–2367.
43 H. Wang, X. Xu and A. Neville, *RSC Adv.*, 2021, **11**, 26273–26283.
44 R. Aggarwal, D. Saini, R. Mitra, S. K. Sonkar, A. K. Sonker and G. Westman, *Langmuir*, 2024, **40**, 9855–9872.
45 M. Saliba, J. P. Atanas, T. M. Howayek and R. Habchi, *Nanoscale Adv.*, 2023, **5**, 6787–6803.
46 R. Quirós-Ovies, M. Laborda, N. M. Sabanés, L. Martín-Pérez, S. M.-D. Silva, E. Burzurí, V. Sebastian, E. M. Pérez and J. Santamaría, *ACS Nano*, 2023, **17**, 5984–5993.
47 Y. Zhuo, I. A. Kinloch and M. A. Bissett, *ACS Appl. Nano Mater.*, 2023, **6**, 18062–18070.
48 P. Chavalekvirat, P. Nakkiew, T. Kunaneksin, W. Hirunpinyopas, W. Busayaporn and P. Iamprasertkun, *Inorg. Chem.*, 2023, **62**, 12851–12861.